ANNALS OF GEOPHYSICS, 69, 2026; doi:10.4401/ag-9409
OPEN ACCESS

Improved Aftershock of the 2006 Yogyakarta M_W ~6.4 Earthquake Sequence Using Deep Learning and Its Correlates with Tectonic Setting

Abraham Arimuko[*,1,2], Po-Fei Chen[1], Yopi Serhalawan[1,2,3], Eko Sujarwanto[4]

(1) National Central University, Department of Earth Sciences, Taoyuan, Taiwan
(2) Badan Meteorologi Klimatologi dan Geofisika, Jakarta Pusat, Indonesia
(3) Academia Sinica, Taiwan International Graduate Program, Earth System Science Program, Taipei, Taiwan
(4) Universitas Siliwangi, Department of Physics Education, Tasikmalaya, Indonesia

Article history: received Juli 17, 2025; accepted March 11, 2026

Abstract

The 2006 Yogyakarta M_W ~6.4 earthquake epicenter was located near the Opak Fault, but slightly farther east, with aftershocks also spreading more toward the east of the fault. The distribution of aftershock did not align precisely with the Opak Fault, raising questions about whether the mainshock originated from the Opak Fault or from another nearby fault. One hypothesis suggests that an eastward dipping fault caused the eastern distribution of the aftershocks. However, the previous studies by Saputra et al. (2021) and Ramdhan et al. (2025a, b) concluded that the M_W ~6.4 earthquake had a westward dipping fault, located to the east of the Opak Fault. In this study, we applied a deep learning method to analyze the arrival times of P and S waves, providing more consistent results than previous approaches. This method has not previously been applied to the analysis of the Yogyakarta M_W ~6.4 aftershock sequence. We used the arrival times of P and S waves to determine the locations and local magnitudes (M_L) of aftershocks. First, we used the grid-search method to determine the absolute hypocenter locations. Then, we updated the velocity model and relocated the events to better represent the seismic conditions in the region. Finally, we selected events to refine the distribution pattern and understand the tectonic setting around the mainshock. The results show that aftershocks in the eastern part of the study area occurred at greater depths compared to those on the western side. To further understand this pattern, we calculated Coulomb stress changes using the focal mechanism from the Global CMT, which aligns with the USGS catalog. The analysis reveals that the shallower earthquakes on the western side of the fault correlate with areas of positive Coulomb stress change. These findings suggest that the 2006 Yogyakarta earthquake was likely triggered by a westward-dipping fault associated with the Ngalang Fault.

Keywords: Opak Fault; Aftershock; Hypocenter; Deep learning; Coulomb stress change

1. Introduction

Yogyakarta is in the middle southern part of Java Island and faces the Indian Ocean. Geodetic analyzes reveal that the Indian Ocean Plate undergoes relative northward motion, with the average slip rate decreasing from ~65 ± 0.4 mm/year in the southern region of Bali to ~58.3 ± 0.5 mm/year along the western part of the trench, highlighting spatial variability in convergence across the Sunda subduction zone (Koulali et al., 2017). Subduction in southern Java contributes to stress transfer to faults on Java Island that accommodate plate motion, one of the faults is the Opak Fault. The Opak Fault is a mapped fault that is in Yogyakarta Province because this fault is also represented as the Opak River, which has a northeast-southwest orientation (Rahardjo et al., 1995) and has already been mapped by the Geological Agency of Indonesia (Badan Geologi). On May 27, 2006, an earthquake occurred at 05:54 am, local time (22:54 UTC) on May 26, 2006, with a magnitude of M_W ~6.4 at a depth of 12.5 km based on parameters issued by the USGS. During the period of this earthquake, the seismic network was not yet very dense even though additions had been made after the Aceh tsunami on December 26, 2004, so that BMKG reported the Yogyakarta earthquake with a local magnitude of M_L 5.9, located on the south coast approximately 20 km from Yogyakarta.

The impact of the Yogyakarta M_W ~6.4 earthquake in 2006 was very severe. Based on reports from the USGS Report (https://earthquake.usgs.gov/earthquakes/eventpage/usp000ej1c/impact), at least 5,749 people were killed, 38,568 were injured, and 127,000 houses were destroyed. This was inseparable from the intensity of the shock, which reached IX on the MMI scale based on responses that filled the questionnaire in the USGS earthquake catalog https://earthquake.usgs.gov/earthquakes/eventpage/usp000ej1c/executive. But the worst damage was not only in areas that were located near the epicenter. The strongest shocks occurred in areas with relatively thick sediment depths that were 10-20 km away to the west relative to the epicenter. The effect of wave amplification caused by the volcaniclastic sediments underneath resulted in strong shocks based on a study by Walter et al. (2008). On the other hand, the directivity of the main earthquake also amplified the shocks (Pawirodikromo, 2012).

The Yogyakarta 2006 M_W ~6.4 earthquake was related to the Opak Fault because of the parallel line, but the surface rupture was offset to the eastern side of the mapped Opak Fault (Tsuji et al., 2009). The source study done by Saputra et al. (2021) found that the earthquake occurred on a west-dipping fault, using the initial point source from USGS to obtain the finite fault solution. The finite fault results were also validated with 524 aftershocks to analyze the slip distribution. The aftershocks were analyzed using hand-picking from a temporary seismic network. The installation of this network aims to record aftershocks to add data sources that can be analyzed because at that time there was no dense sensor distribution. Data from the installation of this seismic network have also been processed for the analysis of the distribution pattern of aftershocks from the results of earthquake localization to the determination of the earthquake location. Furthermore, we relocate the aftershock to refine the hypocenter distribution.

There are publications analyzing 3-dimensional velocity profile anomalies from tomography studies that utilize the recording of P and S wave arrival times in a temporary network (Diambama et al., 2018; Librian et al., 2024). Diambama et al. (2018) and Librian et al. (2024) used 588 and 2,170 aftershock events, respectively, but all relied on hand-picking to determine the P and S wave arrival times (Fig. 1). There are differences in the results of identifying the dipping direction from the source of the Yogyakarta M_W ~6.4 earthquake, which was located 10 km east of the Opak Fault: an eastward dipping orientation was proposed (Diambama et al., 2018), and a westward dipping orientation was named the Ngalang Fault (Librian et al., 2024). The aftershock distribution and dynamic stress transfer results further suggest that the aftershock distribution is associated with the Ngalang Fault, which is located east of the Opak Fault (Ramdhan et al., 2025a).

Although many publications have used the temporary network data, only Sani et al. (2025) determined the arrival times of P and S waves for Yogyakarta M_W ~6.4 aftershocks using machine-learning auto-picking and resulting 2,223, with a limited analysis of the tectonic setting. In our study, the processing is more comprehensive due to using deep learning model, calculating the magnitude, determining the local velocity, and relocating to refine the aftershock sequence's pattern. The use of deep learning for P and S wave analysis speeds up data processing time and provides more consistent picking results (Sun et al., 2023). In addition, the method of determining the arrival time of P and S waves using machine learning is also carried out in the identification of small earthquakes, even microseismic events (Anikiev et al., 2023). In the case of the Yogyakarta earthquake, no one has analyzed the magnitude values of all aftershocks that have been successfully identified.

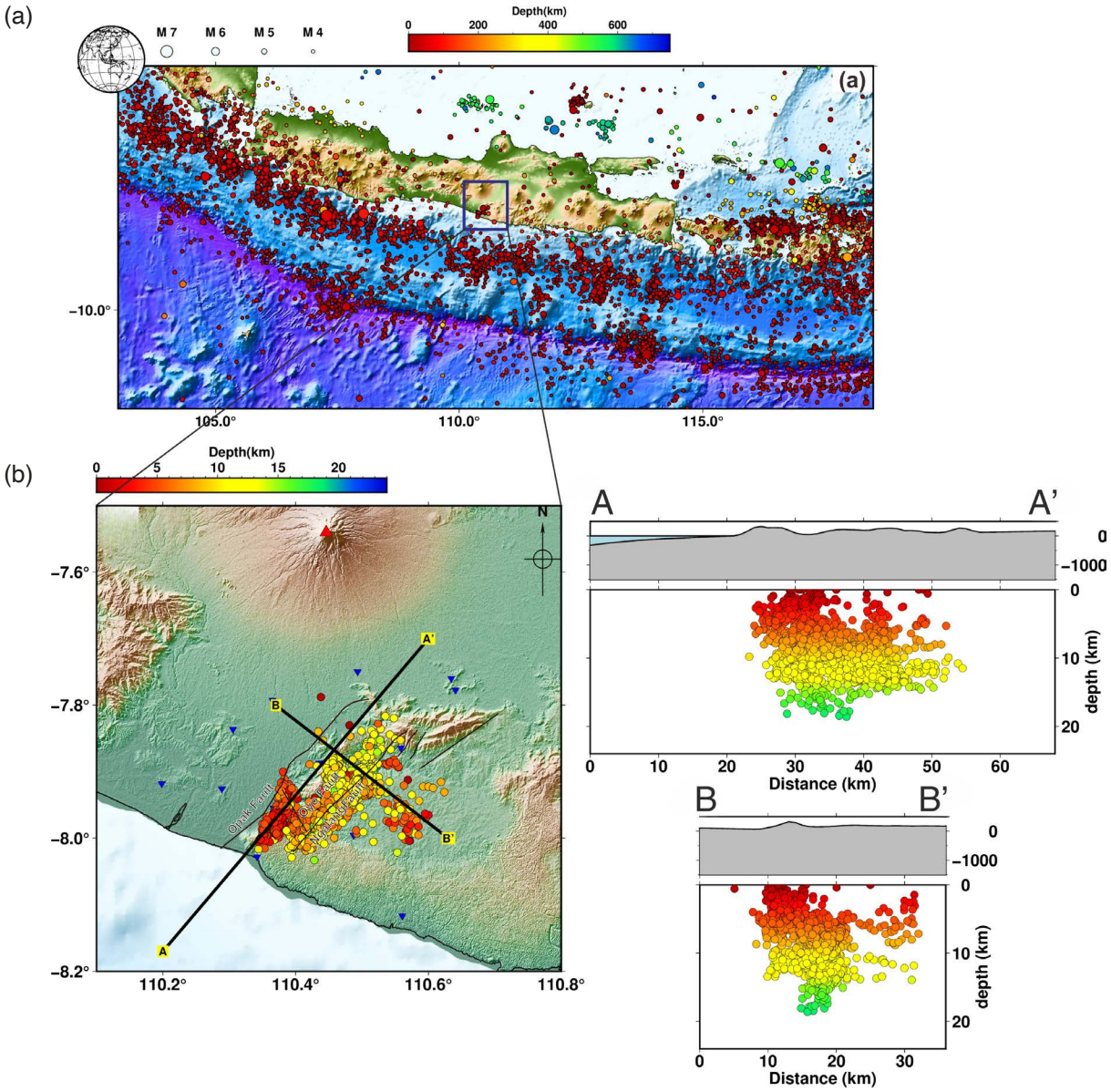

Figure 1. Seismicity map in Java Island and surroundings. (a) Seismicity $M_W \geq 4$ of Yogyakarta from 2008 until 2024, which was obtained from BMKG catalog (https://repogempa.bmkg.go.id/eventcatalog). (b) Earthquake distribution and fault structures from Librian et al. (2024), whose phase arrivals were determined by hand-picking. Moreover, line A-A′ and line B-B′ are parallel and perpendicular to fault structures, respectively.

We used the P and S arrival times from deep learning auto-picking to obtain absolute hypocenter locations. To obtain a more accurate earthquake distribution that can be correlated with geological features, we updated the velocity model to a local one by considering the distribution of the seismic recording network. Then, we use double-difference method to refine the pattern of the hypocenter distribution and geological features. This was done by selecting hypocenters located as earthquake cluster by considering the distribution of aftershock and reducing the residual value by considering other nearby earthquakes. Finally, we calculated the magnitude of all the aftershocks using the P and S phase amplitude information, an approach not utilized in previous work. The results we get are compared with the hand-picking results from Librian et al. (2024). Moreover, we compare the magnitude value results with few aftershock data whose magnitudes have been successfully identified such as from Librian et al. (2024) and Saputra et al. (2021), also with international earthquake monitoring agency, e.g. International Seismological Centre (ISC) and the US. Geological Survey (USGS). Furthermore, we identified the stress transfer distribution pattern by considering the existence of source and receiver faults, which had not been performed in previous work.

2. Data and Preparations

GFZ stands for Geo-Forschungs Zentrum (Geo-research Centre) Germany, installed a temporary seismic network coded XN with 16 seismic sensors to identify more aftershocks of the 2006 Yogyakarta M_W ~6.4 earthquake (Fig. 2). This network used three-component sensors with a sampling rate of 100 Hz. The temporary network was deployed on June 3rd-17th, 2006. We found that the recording condition was not as good as in Fig. 2. We checked and did preprocessing of the waveforms, and we found that not all the stations were able to record the waveforms, probably because of the power supply issue for several days. Some stations had issues with the quality of the seismic recorders, resulting in signals with spikes and gaps.

We downloaded the waveform data in MiniSEED format along with the instrument response data in XML format. Since the response files are in XML, we first converted them into dataless SEED format. Then, we added header information to the MiniSEED files using the rdseed program, resulting in full SEED format. We then extracted the

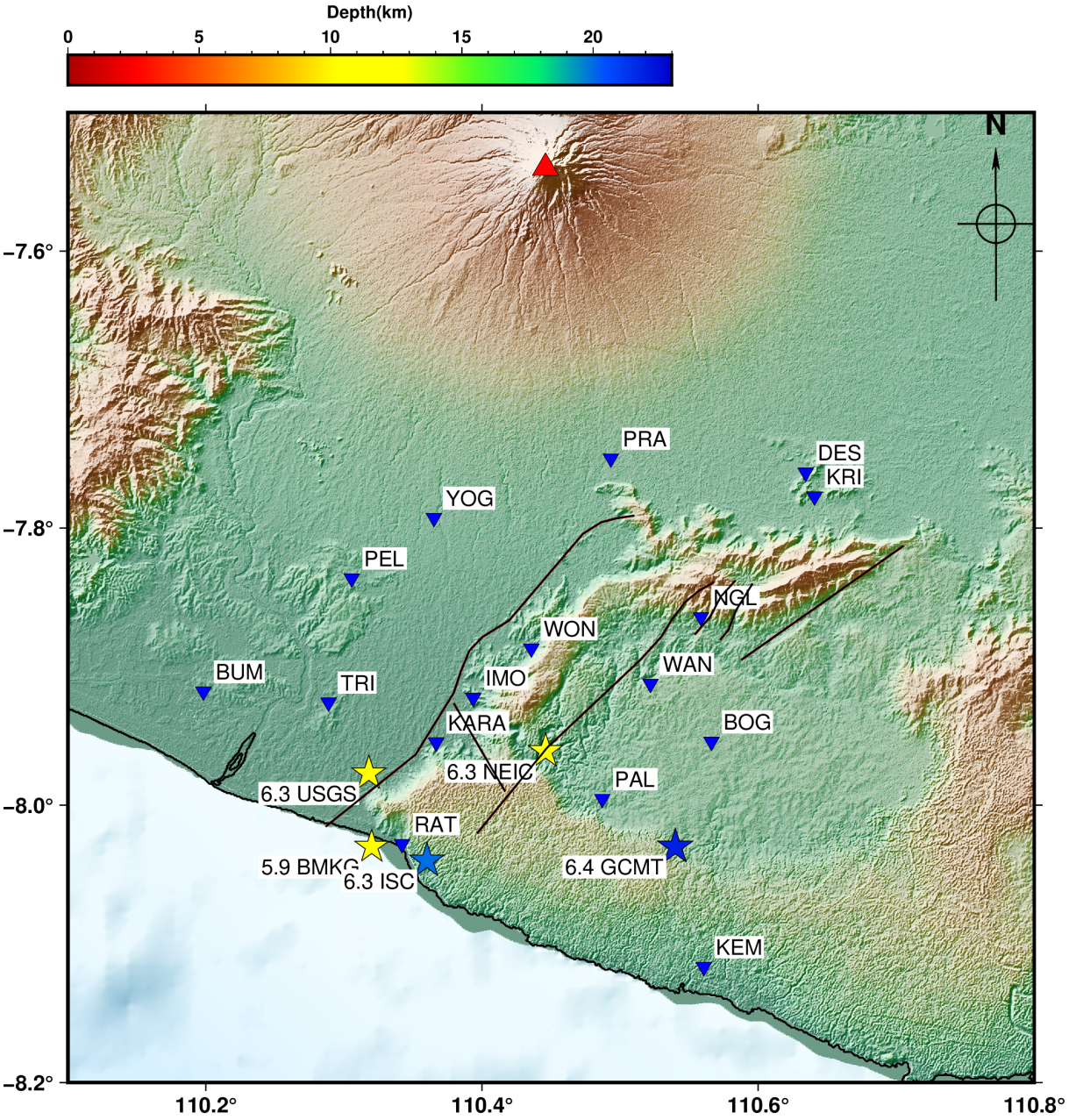

Figure 2. Distribution of 16 temporary seismic networks that were deployed by GFZ. The colored stars are Yogyakarta M_W ~6.4 epicenter from different agencies and earthquake monitoring centers. The black lines are fault models that are proposed by Librian et al. (2024).

waveform data into Seismic Analysis Code (SAC) format using rdseed. After that, we deconvolved the instrument responses (SACPZ) from the waveform (SAC) and added the instrument responses from the Wood-Anderson (WA) seismograph using Bormann (2002) guidelines. The addition of the WA instrument responses was done to meet the requirements for determining the local magnitude (Hutton and Boore, 1987). The example of waveforms with the Wood-Anderson instrument response is in Fig. 3.

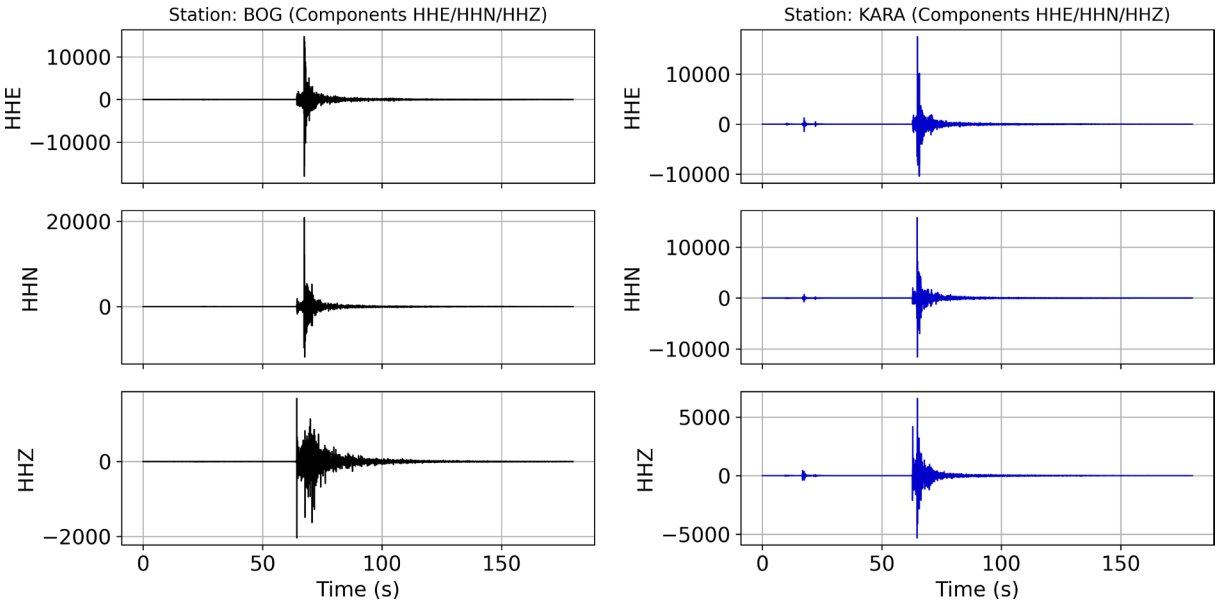

Figure 3. Plot waveforms on BOG and KARA stations on June 16, 2006. We set the start time of the plot to 19:10:42 and plot it relative to the start time to 19:13:42 UTC.

3. Methods

3.1 Earthquake Location Strategy

Hand-picking method to analyze the arrival time of seismic phases has been implemented since the seismograph is able to record the seismic wave. Variability in operators' selection of arrival times introduces inconsistencies that compromise the reliability of manual picking. Consequently, expert validation through waveform analysis is required to ensure methodological rigor and data quality. Technological advancements in seismology have accelerated following the implementation of artificial intelligence (AI), particularly in the automated picking of P- and S-waves, due to its consistency in analysis. But the AI model has to be trained with high quality arrival time picking. PhaseNet is one of the successful algorithms that was built by Zhu and Beroza (2018) using a hand-picked database from the San Andreas seismic network monitoring. The database is used to train a model capable of picking P- and S-wave arrival times, employing a deep neural network methodology. This model has been trained using noise data with a small magnitude that occurred in the high seismicity area in the western part of the United States of America. PhaseNet has been successfully implemented to determine the P and S arrival phases of earthquakes in Northern California (Zhu and Beroza, 2018). The model was not derived from our own training data processing because we did not hand-pick the data, which left us with no input data to train a new model. Instead, we used the available model from Zhu and Beroza (2018), which was trained on data from a tectonic setting similar to Yogyakarta and utilized seismic sensors distributed less than 100 km apart.

We compute the hypocenters using a grid search for absolute location. To perform the earthquake location determination, we implemented the REAL (Rapid Earthquake Association and Location) algorithm from Zhang et al. (2019). This algorithm requires phase-picking results that can be obtained using PhaseNet. We select the P- and S-waves which have picking confidence at least 0.5, same as the criteria that are used by Zhu and Beroza (2018). The hypocenter determination uses a homogeneous half-space layer but considers travel time using a 1D velocity

Table 1. 1-D P and S velocity model in the central of Java (Koulakov et al., 2007).

Depth (km)	v_P (km/s)	v_S (km/s)
0	4.30	2.49
3	4.90	2.83
8	5.70	3.29
16	6.90	3.99
24	7.10	4.10
31	7.50	4.20

model input. We use the average P- and S-wave velocity from Koulakov et al. (2007) as the regional velocity model in our study area. The velocity for P- and S-waves in each layer is shown in Table 1. In determining the hypocenter location using the 3-D grid search method, we defined a spatial extent of 0.3° × 0.3° for longitude and latitude, and 30 km for depth. Subsequently, increments of 0.02° × 0.02° were applied for longitude and latitude, with a depth increment of 0.5 km.

In the initial calculation of the earthquake location, the layered velocity model was not considered to simplify the determination of earthquake location. The VELEST code (Kissling et al., 1994) was implemented to update the velocity model and relocate the hypocenter of the Yogyakarta M_W ~6.4 aftershock sequence. The VELEST algorithm performs a simultaneous (coupled) determination of both the hypocenter and the 1D local velocity model (Kissling et al., 1994) using an iterative approach. Then, we perform a back inversion process to refine the velocity model, which is subsequently used to obtain the relocated hypocenters as an earthquake catalog from a coupled-hypocenter determination method based on the updated velocity model.

Since the aftershock distribution did not align enough with geological features, we performed additional relative hypocenter relocation. To select the aftershock distribution and geological features surrounding the mainshock

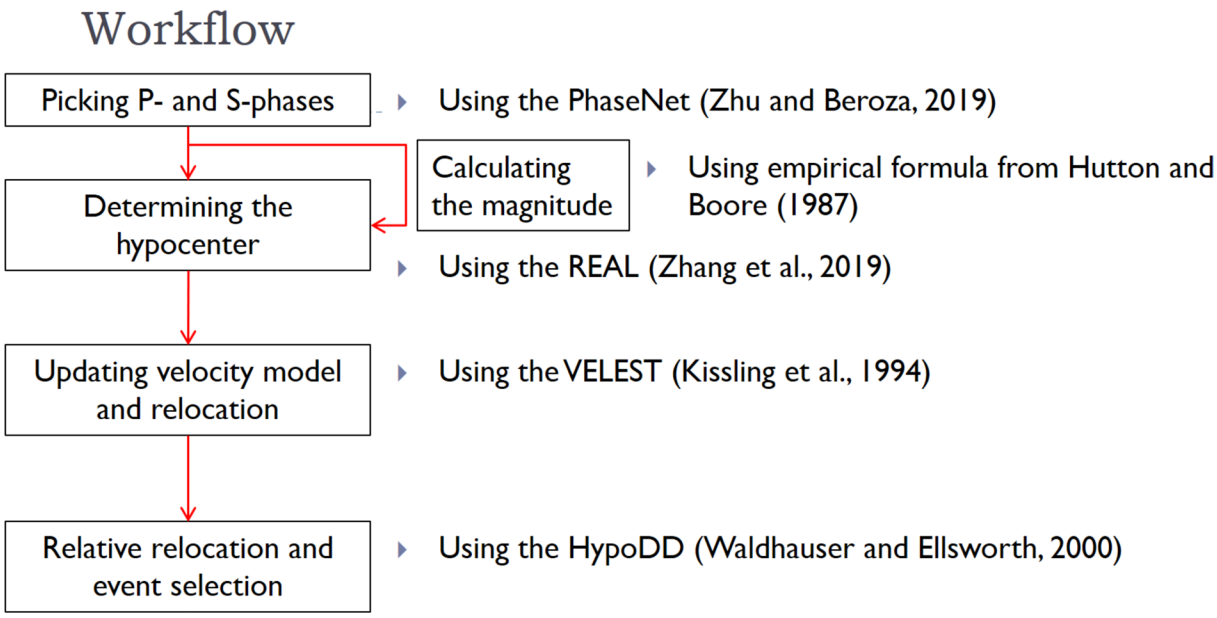

Figure 4. The workflow we followed to determine the aftershock catalog for the 2006 Yogyakarta M_W ~6.4 earthquake.

fault plane, we applied the HypoDD algorithm from Waldhauser and Ellsworth (2000). This method, called the double-difference relocation method, is used to refine the hypocenter distribution that can indicate the correlation with the fault structures. The hypocenter of an earthquake is relocated by considering the earthquake neighbors around it, or it can be said that this calculation is relative to the nearest neighbors. There are several parameters used to determine the relocation hypocenter, such as the distance and the minimum number of earthquakes in one cluster for stable and efficient computational purposes. We use earthquake event selection with criteria of maximum distance between event pair and station 200 km, maximum distance between hypocenter 10 km, minimum number of neighbors 7 earthquakes, with minimum and maximum links of earthquake pair 7 and 50, respectively. In this criterion, we try to maintain as many selected earthquakes as possible and only eliminate those with a sparse distribution. The workflow we utilized is presented in Fig. 4 for clarity. The refined earthquake distribution from this step becomes an earthquake catalog that is used for the interpretation of the tectonic setting surrounding the mainshock hypocenter.

3.2 Calculating Local Magnitude (M_L)

In the subsequent process, while simultaneously determining the hypocenter, the earthquake magnitude is also calculated. To calculate the magnitude, we use the information of P and S-wave amplitudes that were already added with the Wood-Anderson correction during the data pre-processing. The P and S-wave amplitudes are automatically obtained from deep learning auto-picking. We use this approach to determine the local magnitude of the earthquake straightforwardly. Local magnitude has been chosen because this process uses the dense local seismic network. We use the empirical equation of Hutton and Boore (1987) to determine the local magnitude because there is no available local magnitude formula for Indonesia. There is probability a P-wave amplitude higher than S-wave, due to that, we consider the higher amplitude in three components between P- and S-phases in every station. The final magnitude is obtained from the mean magnitude in each station. The magnitude determination was implemented in C language and added to the REAL program. This equation considers the instrument response of the Wood-Anderson seismograph and also the hypocenter distance relative to the recorder seismic stations.

3.3 Coulomb Stress Change Analysis

Earthquake events with magnitudes greater than 4 can result in aftershocks (Elst and Shaw, 2015). Earthquakes can cause aftershocks due to static stress changes (King et al., 1994). The mechanism of the Yogyakarta earthquake is strike-slip, so we use a friction coefficient value of 0.4 based on Toda et al. (2011). Using a basic Coulomb friction model for earthquakes, the potential slip will either increase or decrease at the Coulomb failure stress, which is as follows (Toda et al., 2005):

$$\Delta CFF = \Delta\tau + \mu_s \Delta\sigma_e \tag{1}$$

with ΔCFF is the Coulomb failure, $\Delta\tau$ is the shear stress, μ_s is the friction coefficient, and $\Delta\sigma_e$ is the sum of the normal stress (σ_n) and the fluid pore pressure (P).

Pressure changes occur on nearby or adjacent faults when a fault causes an earthquake. The potential for slip increases and decreases when $\Delta CFF > 0$ and $\Delta CFF < 0$, respectively. The earthquake size, regional stress orientation, assumed friction coefficient value, fault geometry and slip distribution, and other factors all influence the extent to which an earthquake causes ΔCFF. There are several instances where uncertainty in slip distribution dominates the uncertainty in ΔCFF.

We considered the Yogyakarta M_W ~6.4 earthquake from the Ngalang Fault as a source fault, which is located on the eastern side of the Opak Fault. Based on the findings of Librian et al. (2024), we considered two other faults, the Opak Fault and the Oyo Fault, as receiver faults. Using this information, we simulated the stress transfer from the Ngalang Fault to these two receiver faults. While Ramdhan et al. (2025a) conducted a stress transfer analysis, our specific source and receiver fault models had not been previously modeled.

4. Results

4.1 Earthquake Location

In 15 days, the deep learning model was able to identify P- and S-phases in a total of 818,308 phases. To identify the P and S phases, we used three-component waveforms. Then, we obtained 313,040 P- and 254,946 S-picks by selecting the results with the confidence score that were determined through PhaseNet model's prediction probability larger than 0.5. An example of automatic picking is shown in Fig. 5. In the context of local earthquakes, the P wave typically displays a smaller amplitude relative to the S wave (Bormann, 2002).

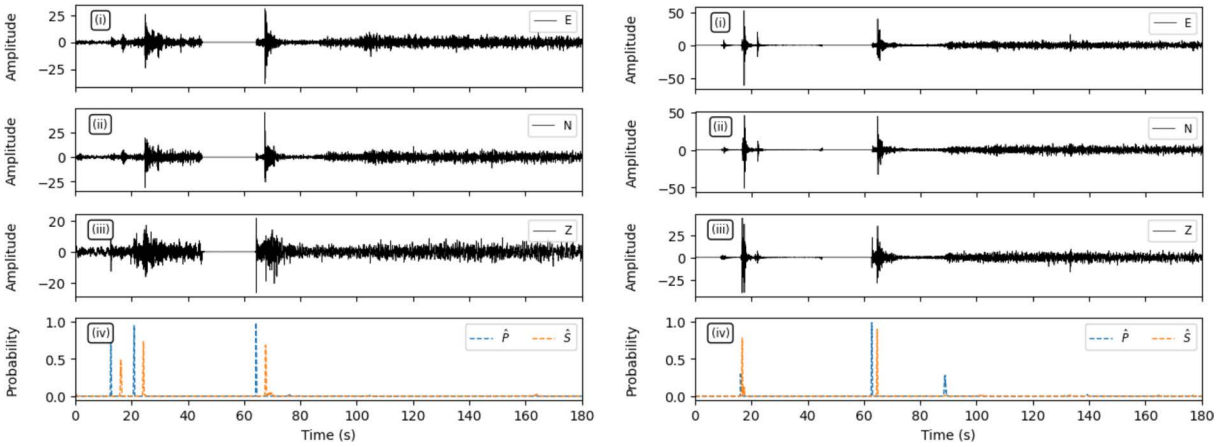

Figure 5. Deep learning picking on station BOG and KARA. The waveforms are the same station and window length as in Fig. 3.

At this stage, two processes are carried out continuously. First, we updated the velocity model to better represent the conditions of the area covered by the seismic network. In this step, we consider the existence of a low-velocity zone surrounding the Opak Fault. Processed earthquake event data are used to simultaneously obtain both the relocated hypocenters and the updated velocity model. We use the arrival time of the P- and S-phases to obtain the minimum residual by damping the origin time, longitude, latitude, depth, and station correction by 0.01, while the velocity is 1.0 with an adjustment of 0.2. The damping for velocity considers 1D regional velocity model (Koulakov et al., 2007) as the initial velocity model is representative of our study area. However, we still use the updated velocity model to perform the relocation because we need a local velocity model that is representative of our study area. In this process, we use 9 iterations with each iteration getting a smaller RMS residual value than the previous iteration. The use of global and local velocity models results in varying percentages of RMS reduction. From first to final iteration there are 57% and 58% for global and local velocity models, respectively. In this process, no earthquakes are eliminated and in total there are 2,923 earthquakes that can be located. The distribution of earthquakes resulting from this procedure is shown in Fig. 6. A comparison of the initial P- and S-wave velocity values from Koulakov et al. (2007) with the updated P- and S-wave velocity models, along with the root mean square (RMS) residuals obtained from both velocity models, is presented in Fig. 7. Moreover, the RMS and residual distribution for each event are shown in Fig. 8. The absolute relocation of 2,923 earthquakes has a mean RMS of 0.09 second, while the relative relocation of 2,205 earthquakes has a mean residual of 0.003 second and an average azimuthal gap of 109.8°.

Despite obtaining relocated hypocenters, the distribution of aftershocks still shows that several earthquakes showed a spare distribution and did not align with fault structures. It is necessary to select events based on relative hypocenter relocation to obtain refining earthquake distribution. This selection aims to obtain an earthquake distribution pattern that better represents the geological structure around the fault plane of the 2006 Yogyakarta M_W ~6.4 earthquake. There are 2,923 events from the REAL catalog which successfully relocated using coupled-hypocenter determination as absolute relocation and they would be relocated using relative relocation as the hypoDD process. We obtained 2,205 events and these earthquake distributions correspond to the tectonic setting.

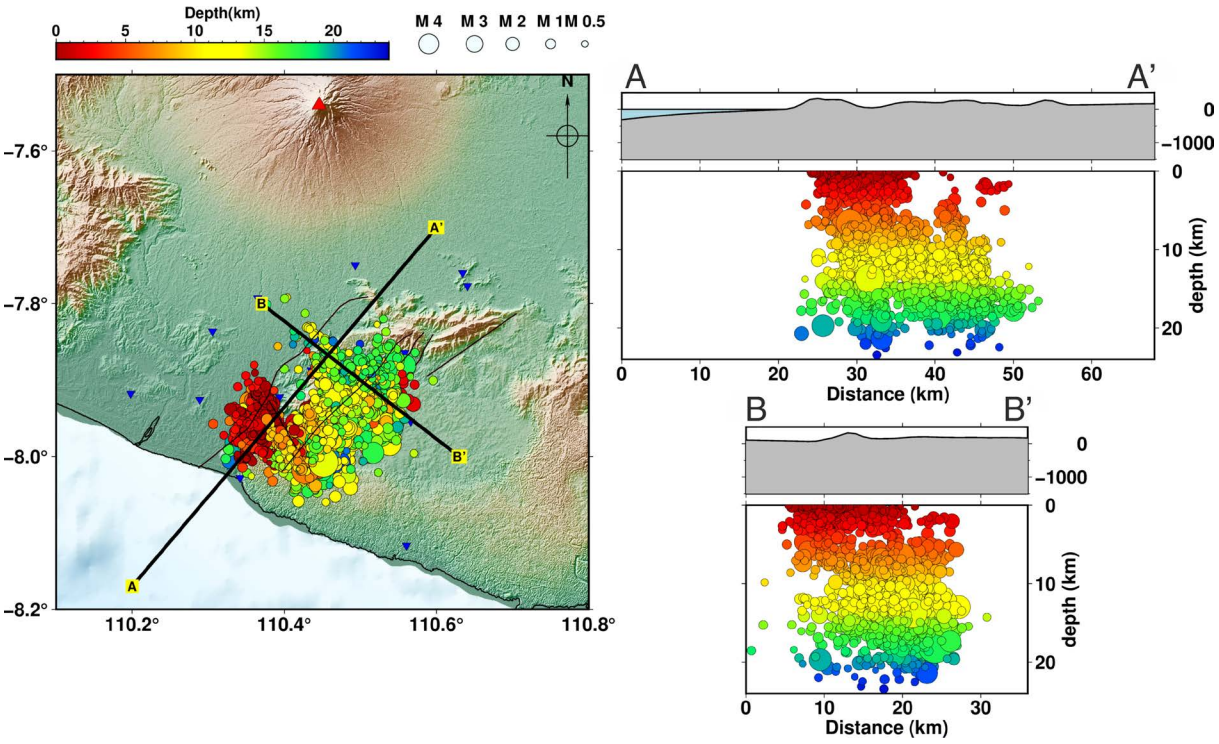

Figure 6. Earthquake distribution from VELEST algorithm. We use the local velocity model that is obtained from updating the Koulakov et al. (2007) 1-D as the initial model.

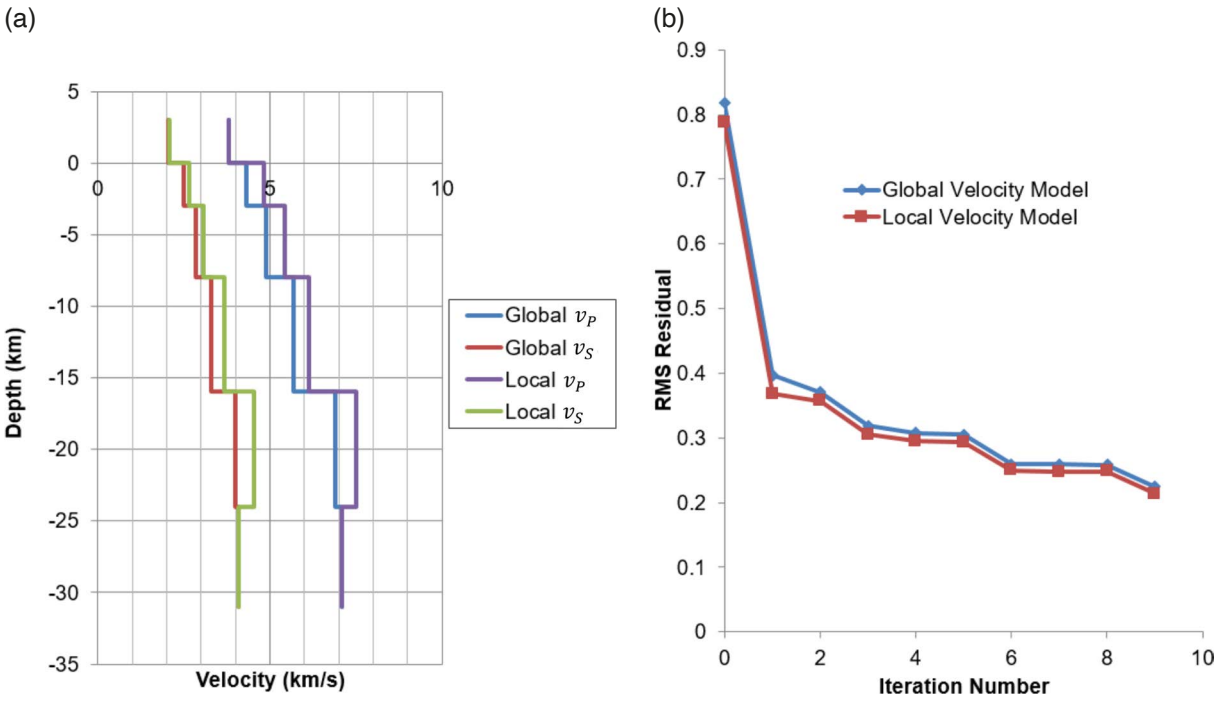

Figure 7. Comparison of the global velocity model (AK135) and local 1-D velocity model that uses 1D regional velocity model (Koulakov et al., 2007) as initial model. (a) Global and local velocity model comparison for v_P and v_S. (b) Misfit in nine iterations in VELEST uses AK135 and an updated velocity model.

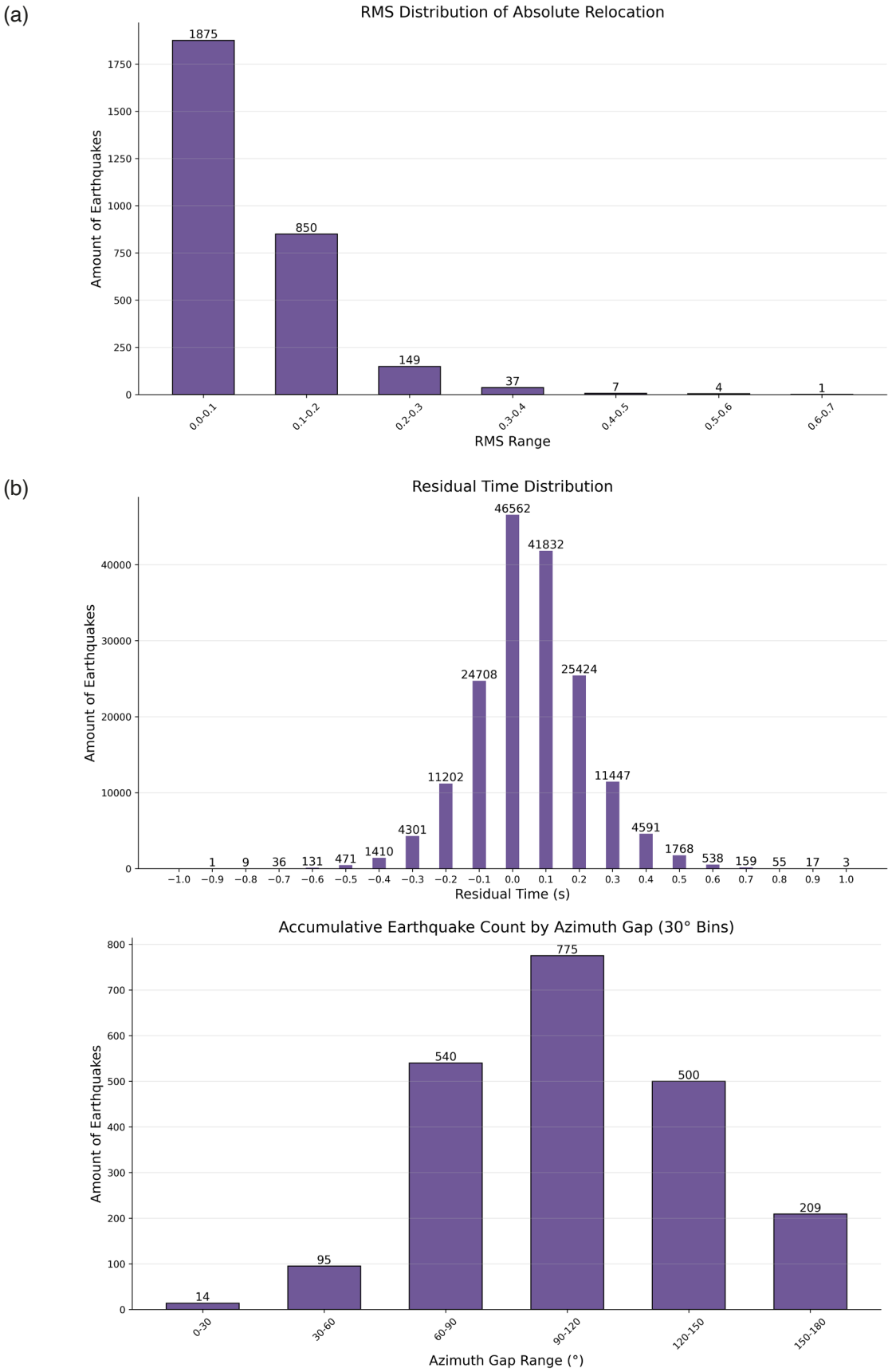

Figure 8. The residual time distribution from all of the aftershocks after absolute and relative relocation. Figure 8a shows the RMS distribution from absolute relocation that uses coupled-hypocenter determination. Figure 8b illustrates the residual time distribution from relative relocation that is conducted in double-difference method. In addition, we also present the azimuth distribution that we obtain from relative relocation.

The distribution of earthquakes after this process is shown in Fig. 9. Most of the earthquake events are located in Ngalang fault as the main fault of 2006 Yogyakarta M_W ~6.4 earthquake.

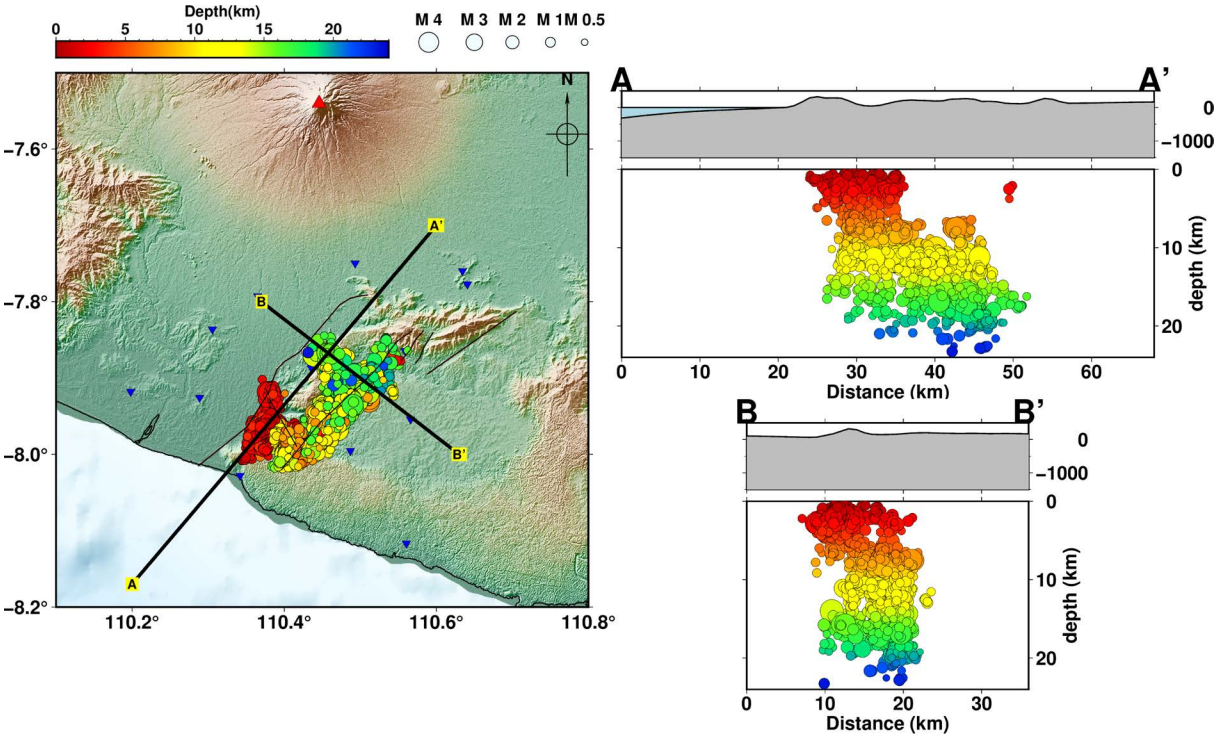

Figure 9. Earthquake distribution from HypoDD algorithm. We use the local velocity model that is obtained from updated 1D regional velocity model (Koulakov et al., 2007) as initial model.

4.2 Magnitude and Coulomb Stress

At this stage, the magnitude was determined immediately after the earthquake's location had been obtained. The earthquake locations are used to determine the distance between hypocenter to the stations. Thus, we obtained a local magnitude value for each earthquake. Figure 10 shows the distribution of earthquake frequency as a function of magnitude. The earthquake magnitude is dominated in range 1.8 to 2.2. The magnitudes calculated for all events in this study represent novel results that have not been reported in previous publications. These findings are significant for delineating seismicity patterns that are closely associated with mapped fault structures. In the absence of comparable magnitude calculations in prior studies, it was not possible to evaluate the overall magnitudes of all earthquake events against earlier published datasets. However, earthquake events documented in previous studies and recorded in the global earthquake catalog, along with their magnitudes, are summarized in Table 2.

The coseismic process of the mainshock generated stress changes that can be identified through variations in static stress values. These variations are controlled by the strike, dip, rake, and slip distribution, which constitute the primary parameters of the earthquake source mechanism. Such parameters are essential for calculating static Coulomb stress on the source fault as well as on nearby receiver faults. In our model, we consider The Ngalang Fault can generate an earthquake M_W ~6.4 with 12.5 km depth as the source fault. Moreover, two other faults, Oyo Fault and Opak Fault have fault dimensions and source parameterization based on the aftershock distribution as receiver faults. These two receiver faults did not use to calculate the static stress change but the fault dimensions are needed to reconstruct the receiver model. The source parameters of three major faults near the mainshock epicenter have been shown in Table 3. Furthermore, we used the scaling law of Blaser et al. (2012) to determine the fault dimensions and slip homogeneity of the Yogyakarta earthquake M_W ~6.4.

We have identified the stress change in the function of depth at 0 km, 7.5 km, 12.5 km, and 17.5 km depths (Fig. 11). The distribution of static stress variations correlates with aftershock location. Most of the aftershock distribution is concentrated in the red zone, or positive stress area, which ranges from 0.2 to 1.0 bar in panels a, b, and d. Even

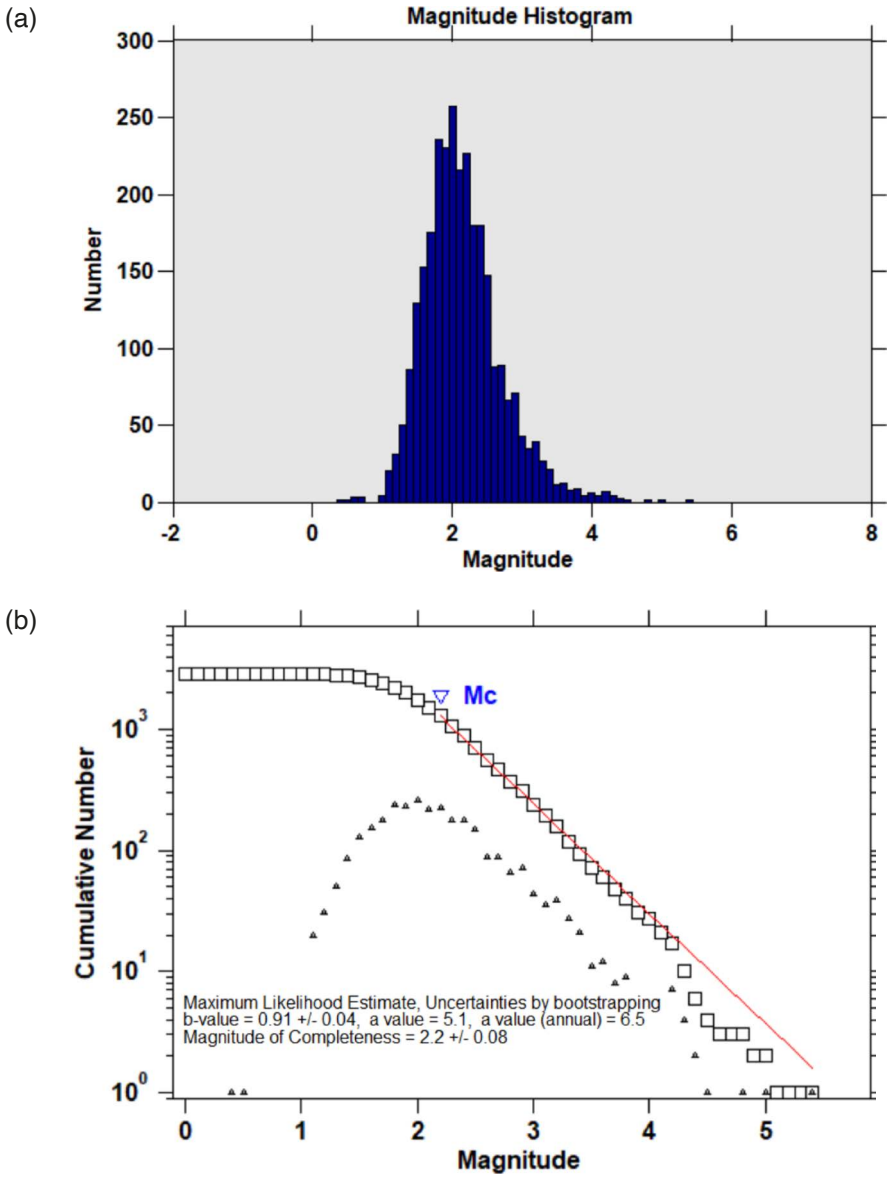

Figure 10. The distribution of earthquake magnitudes from the aftershocks of 2006 Yogyakarta M_W ~6.4 earthquake. (a) The highest number of earthquakes occurred at magnitude M_L 2.1. (b) Across all events, the calculated magnitudes ranged from 0.4 to 5.4, representing the lowest and highest values, respectively, with magnitude of completeness M_L 2.2.

though panel b exhibits a negative Coulomb stress change distribution. This is because when there is a movement in the strike-slip mechanism in the area near the depth of the hypocenter, and we assume a centroid, the greatest stress release occurs when an earthquake occurs (Sato et al., 2012), which releases stress during the coseismic process. The results of our stress transfer model strengthen the correlation between the aftershock distribution pattern and the tectonic setting. The panel c dominantly has a negative stress transfer due to the same as the hypocenter depth. The physical experiment correlates with the fault propagation, explaining the crack and deformation along the fault (Tchalenko, 1970). The strike-slip mechanism releases the stress along the hypocenter depth and also in the shallower depth. Hypocenter distribution in negative Coulomb stress region after significant strike-slip event with depth ≤30 km also happened in the previous study in Japan (Ishibe et al., 2011). This observation aligns with our result, extending up to 5 km shallower than the hypocenter depth.

Table 2. Comparison of aftershock magnitude in the results obtained with previous research and earthquake catalogs of earthquake monitoring institutions.

Date	Time	Mag	Lat	Lon	Dep (km)	Source
2006-06-08	04:44:22.19	M_L 5.4	−7.932	110.4799	13.473	This study
2006-06-09	01:06:45.15	M_L 4.3	−7.9421	110.3899	1.25	
2006-06-16	19:11:42.54	M_L 4.8	−8.0246	110.4202	9.75	
2006-06-17	00:57:00.29	M_L 5	−8.0029	110.4413	16.25	
2006-06-08	04:44:23.72	M_W 4.5	−7.9195	110.4972	13.09	Librian et al. (2024)
2006-06-09	01:06:46.04	M_W 4.6	−7.9483	110.3855	10.16	
2006-06-16	19:11:42.55	M_W 4.6	−8.0063	110.4185	8.81	
2006-06-17	00:57:01.52	M_W 5.0	−7.9863	110.4390	13.42	
2006-06-08	—	M_W 4.2	—	—	15	Saputra et al. (2021)
2006-06-09	—	M_W 4.1	—	—	11	
2006-06-16	—	M_W 4.0	—	—	6	
2006-06-09	01:06:45.00	M_b 4.1	−7.9700	110.4000	10	ISC
2006-06-16	19:11:41.00	M_b 3.7	−8.0700	110.3900	11.8	
2006-06-16	19:11:41.00	M_b 3.7	−7.9500	110.4600	10	NEIC

Table 3. The source parameters to simulate the Coulomb Stress Change.

Fault	Lon (°)	Lat (°)	Length (km)	Width (km)	Strike (°)	Dip (°)	Rake (°)
Ngalang	110.446	−7.961	22.7	8.9	232	86	−13
Oyo	110.394	−7.958	7.2	5.4	317	81	−5
Opak	110.357	−7.954	12.8	7.0	40	58	3

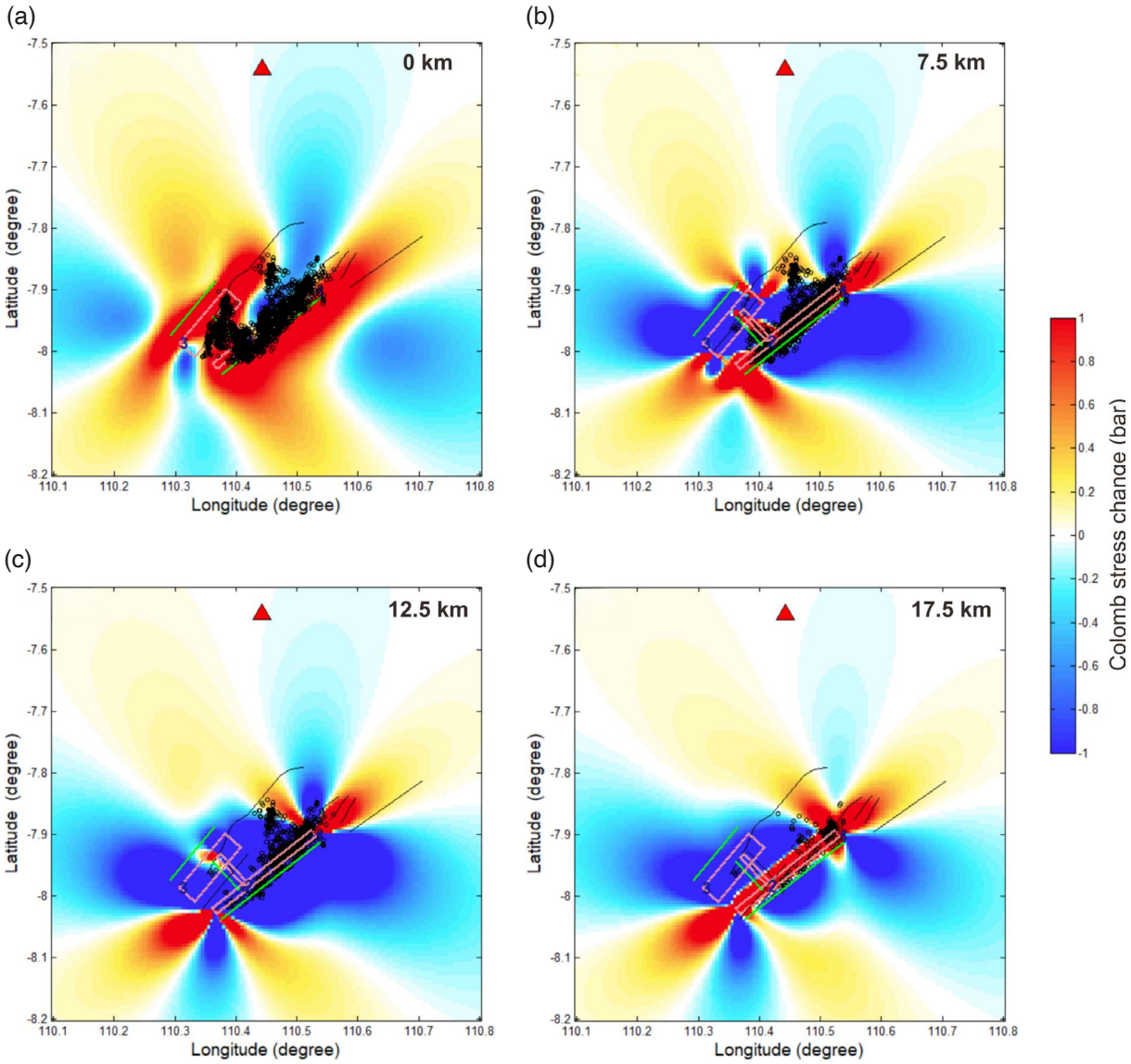

Figure 11. The distribution of Coulomb stress changes in depth. Fig. 11a-d show the distribution at depths of 0 km, 7.5 km, 12 km, and 17.5 km, respectively. The red line at depth is the fault plane and the green line is the projection of the fault plane on the surface. The red triangle indicates the position of the Merapi volcano, the black line is the fault, and the black circle shows the distribution of aftershocks seen at each depth in arrange between those slicing depth to the maximum depth of the aftershock. In details, for Fig. 11a-d, we plot aftershocks from 0-23 km, 7.5-23 km, 12.5-23 km, and 17.5-23 km depth, respectively.

5. Discussion

Earthquake events identified from auto-picked arrival times of P and S waves were validated using an earthquake catalog that was manually picked. This catalog covers the same time span as the auto-picked data. We used the earthquake catalog from Librian et al. (2024), which was developed for subsurface identification through local tomography. An earthquake is considered a match if the residual for its origin time is within ±3 seconds when comparing the hand-picked and deep-learning picked results. A direct comparison between auto-picked and manually picked events yielded a match rate of 80% from the REAL result. The comparison of daily recall values is shown in Table 4. In this study, a tolerance of ±3 seconds is applied when comparing hand-picked phases with automatically detected phases using deep-learning methods, with differences largely determined by the number of phases defining the earthquake and the velocity model adopted for event location. Even though some earthquake locations have moved significantly (as shown in Fig. 12), the RMS and residual times for absolute

Table 4. Comparison results between manual and deep-learning event detection. The results are compared on each day from June 3, 2006, until June 17, 2006.

Date	Unmatch	Match	Hand-pick	REAL	Recall
0603	53	134	187	193	72%
0604	37	121	158	179	77%
0605	48	107	155	157	69%
0606	25	75	100	122	75%
0607	25	88	113	132	78%
0608	31	61	92	88	66%
0609	36	96	132	141	73%
0610	29	158	187	213	84%
0611	24	134	158	231	85%
0612	17	121	138	209	88%
0613	21	121	142	225	85%
0614	33	145	178	226	81%
0615	21	116	137	246	85%
0616	10	129	139	286	93%
0617	13	141	154	275	92%

and relative relocation, respectively, from all aftershocks indicate reliable results, with errors predominantly within 0.1 seconds (Fig. 8).

We also compared the final catalog consisting of 2,205 earthquakes with 2,141 earthquakes hand-picking from Ramdhan et al. (2025a) from the Double-Difference (DD) relocation. In DD relocation, we selected earthquake events to obtain an earthquake distribution that better shows the geological structure associated with the earthquake distribution. The event selection causes the recall rate to 61%. The comparison of earthquake distribution is shown in Fig. 12 with an average difference in earthquake locations between hand and deep learning picking of 3.19 ± 2.49 km, also considering the vertical displacement. The lower recall rate and the maximum location difference of up to 5.7 km between the two catalogs arise from significant variations in the parameters used to determine the origin time and earthquake location. On the other hand, the relocated hypocenters use a Double-Difference method from deep-learning picking, with average uncertainties 0.16 km, 0.18 km, and 0.24 km for latitude, longitude, and depth, respectively. As observed, the earthquake distribution from hand-picking is scattered outside the fault zone and exhibits a shallower dominant depth than the deep-learning results. Although the difference in P- and S-wave arrival times is similar between the two methods, the deep-learning approach identified a greater number of S phases. This increased phase data provides better constraints on the earthquake depth compared to hand-picking.

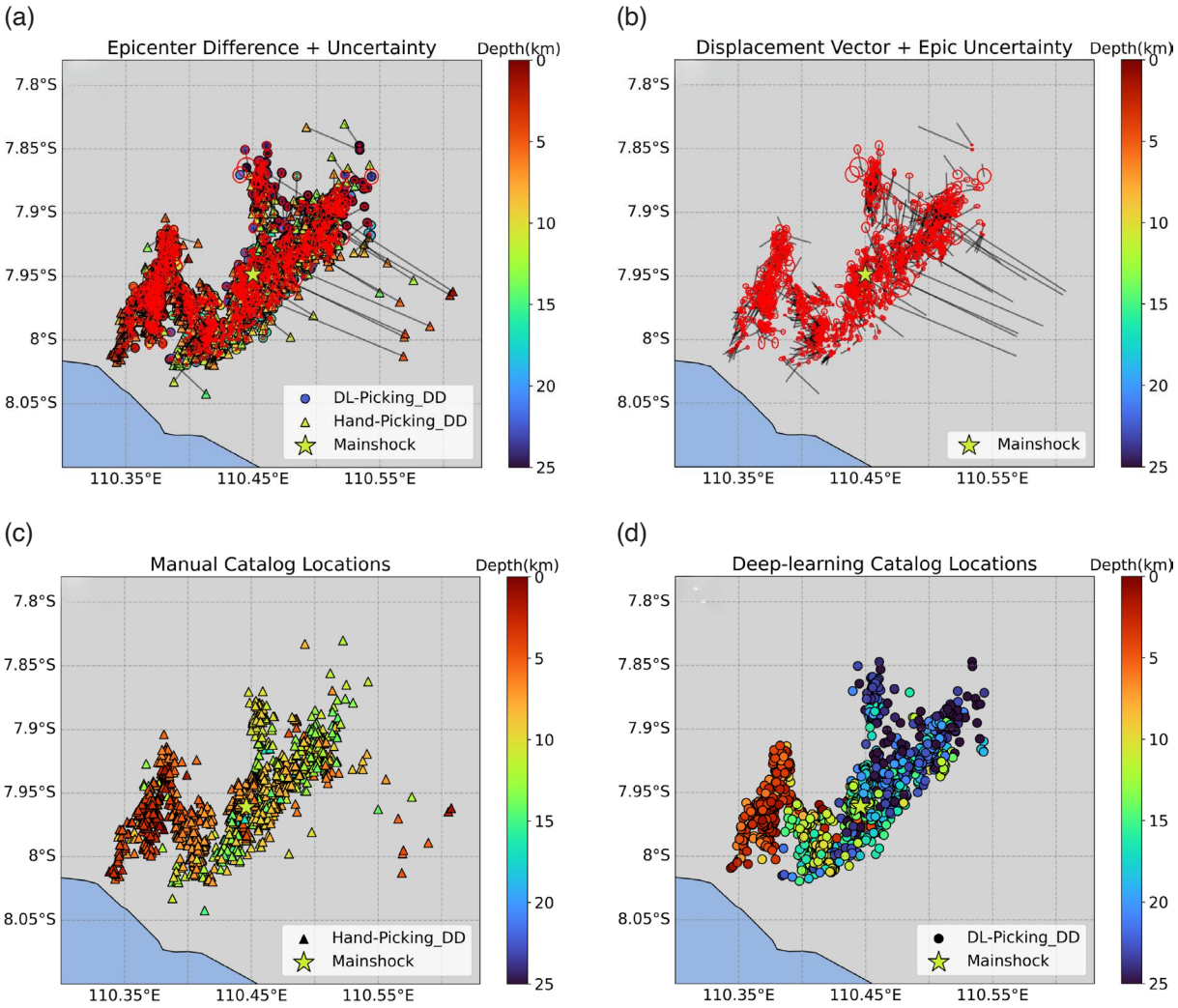

Figure 12. Earthquake distribution from manual and deep-learning locations that are already relocated in the same method. (a) Earthquake event pairs from recall process with origin time different by ±3 seconds. (b) The black line indicates the displacement vector from the relocated hand to deep-learning picking relocation. The red ellipse represents the uncertainty of the deep-learning epicenter. (c) Earthquake distribution from hand picking. (d) Earthquake distribution from deep learning picking.

The magnitude of aftershocks is challenging to calculate and is often overlooked in standard catalogs. This is due to the relatively small amplitude produced, making it more difficult to analyze. However, we have compiled a catalog of aftershocks that includes magnitude information. This will contribute valuable data for the analysis of earthquake clusters in relation to tectonic conditions. Additionally, we compared the magnitude values obtained with those from the previous studies and the global earthquake catalog, such as NEIC (National Earthquake Information Center) and ISC (International Seismological Catalogue) catalogs, as shown in Table 2. Because of the differences in magnitude types, we cannot directly compare the magnitude values of each earthquake. However, the local magnitude (M_L) obtained can be correlated with other magnitude types through regression analysis, although in our case it was not solid enough due to the limited data that contains information of other types of magnitude. We calculated the empirical formula to convert local magnitude (M_L) to moment magnitude (M_W) and body wave magnitude (M_b), as shown in the following equation:

$$M_W = 0.0989M_L + 3.622 \tag{2}$$

$$M_b = 0.3636M_L + 2.1364 \tag{3}$$

This study identifies the smallest local magnitude that can be detected by the temporary network. From the 2,923 earthquake events detected, we obtain a magnitude of completeness (M_L) of 2.2 and a b-value of 0.91 (Fig. 10). By adding a bootstrapping of 100 samples to calculate the uncertainty, the Entire Magnitude Range EMR method (Woessner and Wiemer, 2005) is used to determine the magnitude of completeness. We also spatially identified the distribution patterns of the a- and b-values using aftershock data from the Yogyakarta M_W ~6.4 earthquake (Fig. 13). This pattern indicates a correlation between an increase in the a-value, a decrease in the b-value, and the total number of earthquake events. This is consistent with findings from previous work conducted south of Yogyakarta (Arimuko et al., 2018) and within the subduction zone in the southern segment of West Java (Arimuko et al., 2023), which identified the presence of a seismic gap. A region with low seismicity at the junction of the Opak Fault and Ngalang Fault – which is connected to the Oyo Fault – is an area of high stress release from the M_W ~6.4 main earthquake and indicates the lower b-value with 0.91, as observed from the pattern of negative stress transfer distribution. Conversely, areas with positive stress transfer exhibit high a- and b-values, which are also characterized by a pattern of high seismicity. Thus, we can summarize that positive stress transfer leads to numerous aftershocks, resulting in high a- and b-values.

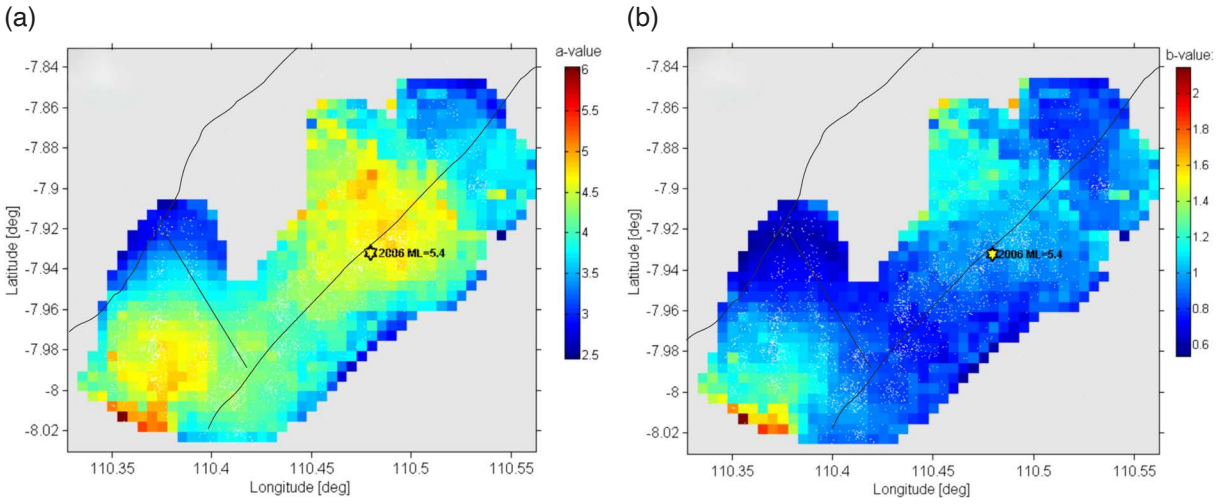

Figure 13. The a- and b-values obtained from aftershock data. (a) The a-value map shows higher values near the location of the highest magnitude event we determined. (b) The b-value map has small values in the area where the Opak Fault and Ngalang Fault meet, which is connected to the Oyo Fault. The yellow star represents the largest magnitude aftershock $M_L = 5.4$.

Earthquake distribution is closely related to geological structures. The significant earthquakes that follow earthquake sequences onshore show numerous aftershocks that are linked to surrounding faults, such as those observed in the 2019 Ridgecrest, California M_W ~6.4 Foreshock and M_W 7.1 Earthquake, several Turkey earthquakes more than M_W 7.0 in 2023 and their aftershocks, and Dapu Earthquake M_W ~6.4 in 2025 (Huang et al., 2020; Zhan et al., 2024; Wu et al., 2025). Significant earthquakes which triggered many aftershocks and proved as newly mapped faults included the Cianjur earthquake (M_W 5.6), the Nusa Tenggara Sea earthquake (M_W 7.3), and a section of the Great Sumatera Fault (M_W 7.2) (Supendi et al., 2022; Supendi et al., 2023a; Supendi et al., 2023b). We identified a geological pattern that provides information about the fault segments surrounding the Yogyakarta M_W ~6.4 earthquake fault plane. This distribution of earthquakes can occur due to static stress transfer from the mainshock to the surrounding fault segments. The stress distribution pattern from the mainshock is illustrated in Fig. 14. With this pattern, we can identify the receiver fault segments of the mainshock, which is further supported by the distribution of the observed aftershocks. Coulomb stress change plotted against depth explains the distribution of aftershocks by considering interactions between faults in complex geological systems, and this has not been discussed in the previous study by Ramdhan et al. (2025a).

Aftershocks are known to occur in regions with increased stress (positive stress zones), according to the analysis of Coulomb stress changes. This means that the area experiences increased stress after the mainshock.

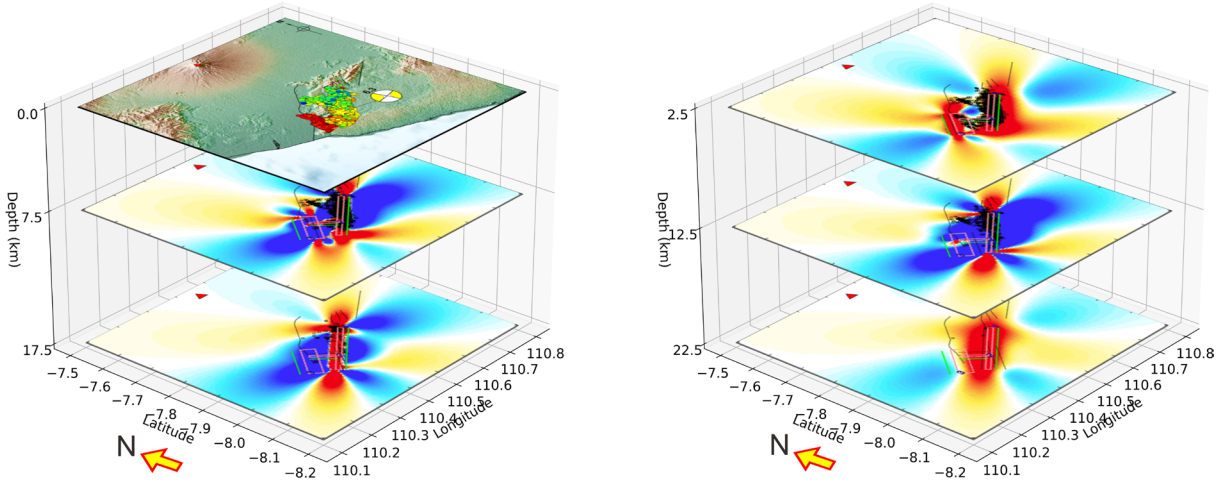

Figure 14. Coulomb stress change distribution corresponding to depth on the fault plane. We plot aftershocks from 0-23 km, 7.5-23 km, 12.5-23 km, and 17.5-23 km depth, respectively. The positive stress regions predominantly occurred on the shallower 7.5 km and deeper 17.5 km depths. In contrast, the negative region of source fault was beginning at 7.5 km and increased to 12.5 km as the hypocenter. After that, the stress on Ngalang Fault as a source fault was having a positive region when the depth changed deeper than hypocenter depth. That we can see at 17.5 km and 22.5 km depth.

Therefore, it suggests that aftershocks were likely triggered by the mainshock. This finding is consistent with earlier research showing that aftershocks typically occur in regions that are more stressed as a result of the mainshock (King et al., 1994; Wu et al., 2017). Regarding the red (positive stress) and blue (negative stress) zones, according to Toda et al. (1998), increased stress in an area will increase seismic activity in that area. In another study, Toda et al. (2012) reported that the blue zone, characterized by lower stress or stress shadow, is associated with a reduced occurrence of aftershocks. The simplification of the fault slip model in this study – specifically, the assumption that the value of slip on the fault plane is uniform – is probably the cause of the aftershocks in the blue zone or locations with lower stress.

The Opak Fault, which has been reported to have an east-dipping orientation (Widijono and Setyanta, 2007), is parallel with the seismicity pattern of aftershocks from the Yogyakarta M_W ~6.4 earthquake (Diambama et al., 2018). To refine the earthquake distribution pattern with the regional tectonic structure around the mainshock, the aftershocks were relocated using the double-difference method to improve the spatial resolution and accuracy catalog (Fig. 15). The distribution along the eastern fault, corresponding to the mainshock fault plane, shows greater depths that become shallower to the west, resulting in what appears to be an eastward-dipping pattern and was interpreted as east-dipping faulting in the previous studies. However, the aftershocks did not occur in a single fault plane.

The seismicity occurred on different faults and can be recognized with the pattern in each fault (Fig. 15). Based on the aftershock pattern, we can design each fault geometry. The magenta rectangle represents the Ngalang Fault as the main fault that generated the Yogyakarta M_W ~6.4 and it matches the pattern with the seismicity. The black rectangle illustrates the Opak Fault that has an east-dipping angle, and in between Ngalang and Opak Fault there is Oyo Fault that has a northeast-dipping angle represented by a white rectangle. The mainshock resulted in a change in Coulomb stress around the Ngalang Fault, leading to elevated stress values along the southern segment of the Opak Fault, which is structurally connected by the Oyo Fault located south of the Ngalang Fault (Ramdhan et al., 2025a).

The absence of a seismic migration pattern strengthens the previous finding, which occurred along the Ngalang Fault and subsequently induced seismic activation along the Oyo and Opak Faults. This may be attributed to transient shear stress generated by the mainshock, which increased stress on the Oyo and Opak Faults through dynamic rupture branching and rupture jumping, respectively (Ramdhan et al., 2025a). The Coulomb stress change distribution reveals a positive anomaly extending both westward and eastward from our finding. Given that the Opak Fault lies to the west, this positive stress triggered shallow seismicity, primarily concentrated at depths shallower than 10 km.

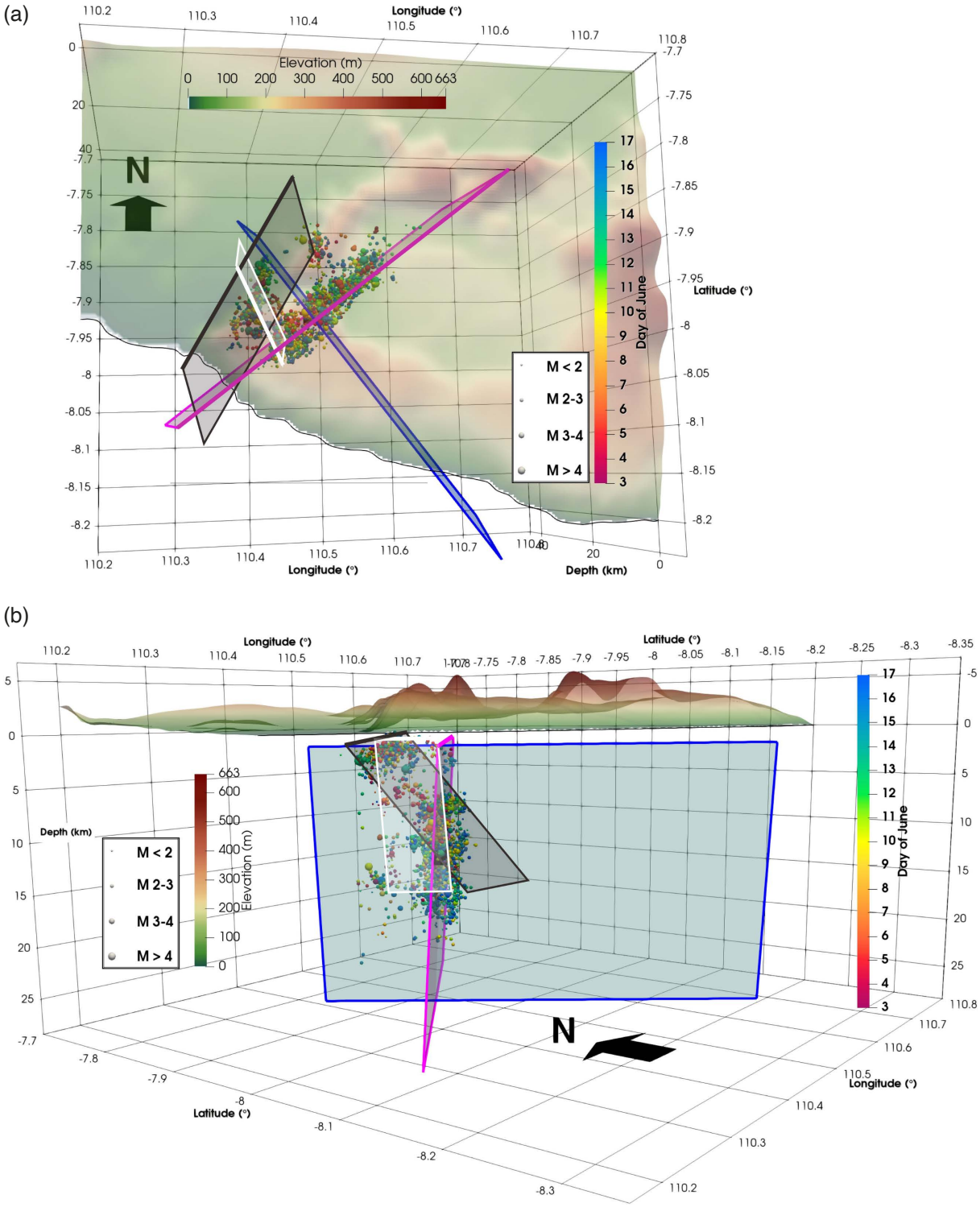

Figure 15. The aftershock distribution from a double-difference method on the nodal plane based on Global CMT is the same as the USGS solution. The size of fault planes is based on the scaling law formula from Goldberg et al. (2022). The blue rectangle is Nodal Plane 1 of Ngalang Fault with strike 323°, dip 77°, and rake −176°. The purple rectangle is Nodal Plane 2 with strike 232°, dip 86°, and rake −13°. The black and white rectangles represent Opak Fault and Oyo Fault, respectively. (a) Map view of aftershock distribution. (b) Cross-section aftershock distribution parallel with the Nodal Plane 1.

6. Conclusions

Auto-picking was conducted using a deep learning approach, which significantly improved the quantity and consistency of hypocenter determinations following the application of relative relocation techniques. Subsequently, static stress change analysis was employed to investigate the spatial distribution of hypocenters, revealing a strong correlation with adjacent fault segments surrounding the mainshock fault plane. Based on our analysis, we obtained conclusions for our study:

1) Deep learning models developed using earthquake data from California have been applied to detect the arrival times of P- and S-phases in the Yogyakarta earthquake sequence. This is supported by the comparison between hand-picked and deep-learning-derived phase picks, which yielded a recall rate of 80.20%, based on 2,170 and 2,923 earthquake events, respectively.
2) We conducted a relocation using the coupled-hypocenter determination method to update the velocity model based on the observed earthquake distribution, followed by a simultaneous relocation of the events. The updated 1-D velocity model, which was derived from a regional 1-D velocity model, has a smaller RMS value compared to using global data. In this process, no earthquake event selection was applied.
3) The magnitude of completeness M_L 2.2 that we obtained in our study fills the gap from the previous studies and indicates the distribution of aftershocks along the Ngalang Fault, Opak Fault, and Oyo Fault. Using the deep-learning catalog, we identified the spatial pattern of a- and b-values, which correlates positively with both stress transfer and the number of earthquake events in each grid. This pattern corroborates previous studies, indicating that the mainshock M_W ~6.4 was accompanied by dynamic rupture branching and rupture jumping.
4) The Yogyakarta M_W ~6.4 earthquake was triggered by a fault on the east side of the Opak Fault that dipped westward and is referred to as the Ngalang Fault, according to the relocated hypocenter from the double-difference method and the distribution of the Coulomb stress change. The aftershock depth on the Opak Fault is relatively shallower than on the Ngalang Fault because the Opak Fault received positive stress at depths between 0 and 5 km.

Data availability statement. The aftershock data obtained from this study are available from the corresponding author, AA, upon request. The seismic data used was collected from the XN temporary network deployed by the GFZ and can be accessed at http://eida.gfz-potsdam.de/webdc3/. The workflow to convert from MiniSEED to SAC available at https://iris-edu.github.io/stationxml-seed-converter/. The PhaseNet package and manual can be downloaded at https://github.com/AI4EPS/PhaseNet.

Competing interests. The authors declare that they have no known competing financial interests or personal relationships that could have appeared to influence the work reported in this paper.

Authors' contributions. AA has processed, interpreted, and written the original and the revised manuscript. PFC has supervised, provided the code, and written the revised manuscript. YS has produced the 3-D figure and analyzed it. ES has written, revisited, and analyzed the manuscript. All authors have agreed to the contents of this manuscript.

Acknowledgements. We want to thank Geo-Forschungs Zentrum (GFZ), and open-source software (QGIS) as well as Generic Mapping Tools (GMT) to produce figures.

References

Anikiev, D., C. Birnie, U. B. Waheed et al. (2023). Machine learning in microseismic monitoring, Earth-Sci. Rev., 239, 104371, doi:10.1016/j.earscirev.2023.104371.

Arimuko, A., F. Yoan, S. Rohadi and K. H. C. Wulur (2018). A-value and b-value as basic calculation seismicity index, repeated period, and vulnerability of earthquakes, in EAGE-HAGI Asia Pacific Meeting on Near Surface Geoscience and Engineering 2018, EAGE, 1-4, doi:10.3997/2214-4609.201800362.

Arimuko, A., S. Rohadi and A. S. Rahman (2023). Seismotectonic Studies to Determine the Recurrence of Earthquakes M_W>7 Using a Statistical Approach and Plate Motion in the Megathrust Western Part of Java, Geotech. Geol. Eng., 41, 1397-1406, doi:10.1007/s10706-022-02342-z.

Blaser, L., F. Krüger, M. Ohrnberger and F. Scherbaum (2010). Scaling relations of earthquake source parameter estimates with special focus on subduction environment, Bull. Seismol. Soc. Am., 100, 6, 2914-2926, doi:10.1785/0120100111.

Bormann, P. and IASPEI (2002). New manual of seismological observatory practice (NMSOP), GeoForschungsZentrum Potsdam, Potsdam, Germany, ISBN:9783980878005.

Diambama, A. D., A. Anggraini, M. Nukman, B. Lühr et al. (2018). Velocity structure of the earthquake zone of the M 6.3 Yogyakarta earthquake 2006 from a seismic tomography study, Geophys. J. Int., 216, 1, 439-452, doi:10.1093/gji/ggy430.

Huang, H., L. Meng, R. Bürgmann, W. Wang et al. (2020). Spatio-temporal foreshock evolution of the 2019 M 6.4 and M 7.1 Ridgecrest, California earthquakes, Earth Planet. Sci. Lett., 551, 116582, doi:10.1016/j.epsl.2020.116582.

Hutton, L. K. and D. M. Boore (1987). The M_L scale in Southern California, Bull. Seismol. Soc. Am., 77, 6, 2074-2094, doi:10.1785/BSSA0770062074.

Ishibe, T., K. Shimazaki, H. Tsuruoka, Y. Yamanaka et al. (2011). Correlation between Coulomb stress changes imparted by large historical strike-slip earthquakes and current seismicity in Japan, Earth Planets Space, 63, 301-314, doi:10.5047/eps.2011.01.008.

King, G. C. P., R. S. Stein and J. Lin (1994). Static stress changes and the triggering of earthquakes, Bull. Seismol. Soc. Am., 84, 3, 935-953, doi:10.1785/BSSA0840030935.

Kissling, E., W. L. Ellsworth, D. Eberhart-Phillips and U. Kradolfer (1994). Initial reference models in local earthquake tomography, J. Geophys. Res. Solid Earth, 99, B10, 19635-19646, doi:10.1029/93JB03138.

Koulakov, I., M. Bohm, G. Asch, G. Lühr et al. (2007). P and S velocity structure of the crust and the upper mantle beneath central Java from local tomography inversion, J. Geophys. Res. Solid Earth, 112, B8, doi:10.1029/2006JB004712.

Koulali, A., S. McClusky, S. Susilo, Y. Leonard et al. (2017). The kinematics of crustal deformation in Java from GPS observations: Implications for fault slip partitioning, Earth Planet. Sci. Lett., 458, 69-79, doi:10.1016/j.epsl.2016.10.039.

Librian, V., M. Ramdhan, A. D. Nugraha, M. M. Mukti et al. (2024). Detailed seismic structure beneath the earthquake zone of Yogyakarta 2006 (M_W ~6.4), Indonesia, from local earthquake tomography, Phys. Earth Planet. Inter., 351, 107170, doi:10.1016/j.pepi.2024.107170.

Pawirodikromo, W. (2012). Seismologi Teknik dan Rekayasa Kegempaan, Pustaka Pelajar, Yogyakarta, ISBN:9786022291107.

Rahardjo, W., Sukandarrumidi and H. M. D. Rosidi (1995). Geologic map of the Yogyakarta quadrangle, Java, scale 1:100,000, Geological Research and Development Center, Bandung, Indonesia.

Ramdhan, M., K. H. Palgunadi, M. M. Mukti, V. Librian et al. (2025a). Aftershock sequence of the Yogyakarta earthquake 2006 (MW ~6.4), Indonesia, based on analysis of hypocenter relocation, static, and dynamic stress, Nat. Hazards, 121, 16559-16579, doi:10.1007/s11069-025-07440-8.

Ramdhan, M., P. Priyobudi, M. M. Mukti, A. S. Putra et al. (2025b). Tracing fault systems from subsurface to surface in Yogyakarta and its surroundings, Indonesia, Nat. Hazards Res., doi:10.1016/j.nhres.2025.07.003.

Sani, A. A., I. Madrinovella, D. A. Zaky and M. Ramdhan (2025). Automatic Seismic Phase Picking and Earthquake Location Using 2006 Yogyakarta Aftershock Datasets Based on A Machine Learning Algorithm, in IOP Conference Series: Earth and Environmental Science, IOP Publishing, 012019.

Saputra, H., W. Wahyudi, I. Suardi, A. Anggraini et al. (2021). The waveform inversion of mainshock and aftershock data of the 2006 M6.3 Yogyakarta earthquake, Geosci. Lett., 8, 9, doi:10.1186/s40562-021-00176-w.

Sato, T., S. Hiratsuka and J. Mori (2012). Coulomb stress change for the normal-fault aftershocks triggered near the Japan Trench by the 2011 MW 9.0 Tohoku-Oki earthquake, Earth Planets Space, 64, 12, 1239-1243, doi:10.5047/eps.2012.04.003.

Sun, H., Z. E. Ross, W. Zhu and K. Azizzadenesheli (2023). Phase Neural Operator for Multi-Station Picking of Seismic Arrivals, Geophys. Res. Lett., 50, 24, e2023GL106434, doi:10.1029/2023GL106434.

Supendi, P., N. Rawlinson, B. S. Prayitno, S. Widiyantoro et al. (2022). The Kalaotoa Fault: A newly identified fault that generated the 7.3 Flores Sea earthquake, Seism. Rec., 2, 3, 176-185, doi:10.1785/0320220015.

Supendi, P., N. Rawlinson, B. S. Prayitno, D. Sianipar et al. (2023a). A previously unidentified fault revealed by the February 25, 2022 (MW 6.1) Pasaman Earthquake, West Sumatra, Indonesia, Phys. Earth Planet. Inter., 334, 106973, doi:10.1016/j.pepi.2022.106973.

Supendi, P., T. Winder, N. Rawlinson, C. A. Bacon et al. (2023b). A conjugate fault revealed by the destructive MW 5.6 (November 21, 2022) Cianjur earthquake, West Java, Indonesia, J. Asian Earth Sci., 257, 105830, doi:10.1016/j.jseaes.2023.105830.

Tchalenko, J. S. (1970). Similarities between shear zones of different magnitudes, Geol. Soc. Am. Bull., 81, 6, 1625-1640, doi:10.1130/0016-7606(1970)81[1625:SBSZOD]2.0.CO;2.

Toda, S., R. S. Stein, P. A. Reasenberg, J. H. Dieterich et al. (1998). Stress transferred by the 1995 $M_W = 6.9$ Kobe, Japan, shock: Effect on aftershocks and future earthquake probabilities, J. Geophys. Res. Solid Earth, 103, B10, 24543-24565, doi:10.1029/98JB00765.

Toda, S., R. S. Stein, K. Richards-Dinger and S. B. Bozkurt (2005). Forecasting the evolution of seismicity in southern California: Animations built on earthquake stress transfer, J. Geophys. Res. Solid Earth, 110, B5, doi:10.1029/2004JB003415.

Toda, S., R. S. Stein and J. Lin (2011). Widespread seismicity excitation throughout central Japan following the 2011 M=9.0 Tohoku earthquake and its interpretation by Coulomb stress transfer, Geophys. Res. Lett., 38, 7, doi:10.1029/2011GL047834.

Toda, S., R. S. Stein, G. C. Beroza and D. Marsan (2012). Aftershocks halted by static stress shadows, Nat. Geosci., 5, 6, 410-413, doi:10.1038/ngeo1465.

Tsuji, T., K. Yamamoto, T. Matsuoka, Y. Yamada et al. (2009). Earthquake fault of the 26 May 2006 Yogyakarta earthquake observed by SAR interferometry, Earth Planets Space, 61, e29-e32, doi:10.1186/BF03353189.

van der Elst, N. J. and B. E. Shaw (2015). Larger aftershocks happen farther away: Nonseparability of magnitude and spatial distributions of aftershocks, Geophys. Res. Lett., 42, 14, 5771-5778, doi:10.1002/2015GL064734.

Waldhauser, F. and W. L. Ellsworth (2000). A double-difference earthquake location algorithm: Method and application to the northern Hayward Fault, California, Bull. Seismol. Soc. Am., 90, 6, 1353-1368, doi:10.1785/0120000006.

Walter, T. R., R. Wang, B.-G. Luehr, J. Wassermann et al. (2008). The 26 May 2006 magnitude 6.4 Yogyakarta earthquake south of Mt. Merapi volcano: Did lahar deposits amplify ground shaking and thus lead to the disaster?, Geochem. Geophys. Geosyst., 9, doi:10.1029/2007GC001810.

Widijono, B. S. and B. Setyanta (2007). Anomali gaya berat, kegempaan serta kelurusan struktur geologi daerah Jogjakarta dan sekitarnya, J. Geol. Sumberdaya Miner., 17, 2, 74-90, doi:10.33332/jgsm.geologi.v17i2.281.

Woessner, J. and S. Wiemer (2005). Assessing the quality of earthquake catalogues: Estimating the magnitude of completeness and its uncertainty, Bull. Seismol. Soc. Am., 95, 2, 684-698, doi:10.1785/0120040007.

Wu, J., Y. Cai, W. Li and Q. Feng (2017). Strong Aftershock Study Based on Coulomb Stress Triggering – A Case Study on the 2016 Ecuador M_W 7.8 Earthquake, Appl. Sci., 7, 1, 88, doi:10.3390/app7010088.

Wu, C. F., R. J. Rau and Y. C. Chen (2025). Fast report: The 2025 Dapu earthquake: Simultaneous rupture of mid-crust antithetic thrust fault linkages in the fold-and-thrust belt of Southwestern Taiwan, Terr. Atmos. Ocean. Sci., 36, 19, doi:10.1007/s44195-025-00101-0.

Zhan, H. L., L. Bai, B. A. Wibowo, C. Y. Liu et al. (2024). The 2023 Turkey earthquake doublet: Earthquake relocation, seismic tomography, and stress field inversion, Earth Planet. Phys., 8, 3, 535-548, doi:10.26464/epp2024022.

Zhang, M., W. L. Ellsworth and G. C. Beroza (2019). Rapid earthquake association and location, Seismol. Res. Lett., 90, 6, 2276-2284, doi:10.1785/0220190052.

Zhu, W. and G. C. Beroza (2018). PhaseNet: A deep-neural-network-based seismic arrival-time picking method, Geophys. J. Int., 216, 1, 261-273, doi:10.1093/gji/ggy423.

***CORRESPONDING AUTHOR: Abraham ARIMUKO**, Department of Earth Sciences, National Central University, Taoyuan, Taiwan Badan Meteorologi Klimatologi dan Geofisika (BMKG), Jakarta Pusat, Indonesia e-mail: abraham.arimuko@bmkg.go.id